Articles in PresS. Am J Physiol Heart Circ Physiol (September 23, 2016). doi:10.1152/ajpheart.00002.2016

Microstructure and mechanics of human resistance arteries

J S Bell[a,c*], A O Adio[b], A Pitt[b], L Hayman[b], C E Thorn[b], A C Shore[b], J L Whatmore[c], C Peter Winlove[a]

[a] Department of Physics, University of Exeter, Stocker Road, Exeter, UK
[b] Diabetes and Vascular Medicine, Institute of Biomedical and Clinical Sciences, University of Exeter Medical School and NIHR Exeter Clinical Research Facility, Exeter, UK.
[c] Institute of Biomedical and Clinical Science, University of Exeter Medical School, University of Exeter, Exeter, UK

*Corresponding author: BellJ10@cardiff.ac.uk
Tel: (+44)1392264140
Fax: (+44)1392264111

Running Head: Microstructure and mechanics of human resistance arteries

Contributions:
JSB designed the myograph, carried out the nonlinear microscopy, analysed the images, wrote the analytical model and drafted the manuscript.
AOA carried out vessel dissection and mounting and assisted with manuscript preparation.
AP assisted in volunteer recruitment and screening and obtained biopsies
LH carried out volunteer recruitment and screening.
CET, ACS and JLW provided supervision and clinical interpretation of results and assisted with manuscript preparation.
CPW provided supervision and physical interpretation of results and assisted with manuscript preparation.

Abstract:
Vascular diseases such as diabetes and hypertension cause changes to the vasculature that can lead to vessel stiffening and the loss of vasoactivity. The microstructural bases of these changes are not presently fully understood. We present a new methodology for stain-free visualisation, at a microscopic scale, of the morphology of the main passive components of the walls of unfixed resistance arteries and their response to changes in transmural pressure. Human resistance arteries were dissected from subcutaneous fat biopsies, mounted on a perfusion myograph and imaged at varying transmural pressures using a multimodal nonlinear microscope. High resolution 3D images of elastic fibres, collagen and cell nuclei were constructed. The honeycomb structure of the elastic fibers comprising the internal elastic layer became visible at a transmural pressure of 30 mmHg. The adventitia, comprising wavy collagen fibres punctuated by straight elastic fibres, thinned under pressure as the collagen network straightened and pulled taut. Quantitative measurements of fibre orientation were made as a function of pressure. A multi-layer analytical model was used to calculate the stiffness and stress in each layer. The adventitia was calculated to be up to ten times as stiff as the media and experienced up to 8 times the stress, depending on lumen diameter. This work reveals that pressure-induced reorganisation of fibrous proteins gives rise to very high local strain fields, and highlights the unique mechanical roles of both fibrous networks. It thereby provides a basis for understanding the micromechanical significance of structural changes which occur with age and disease.

New & Noteworthy:
This is the first study to elucidate and quantify the microstructural bases of the mechanical properties of human resistance arteries. The geometrically-accurate mechanical analysis provides new insights into strain-fields existing in the walls of small arteries, and raises questions about the mechanobiology of vascular remodelling.

Keywords: Resistance artery, Blood pressure, Extracellular matrix, Stress, Mechanical modelling

Introduction

The network of small resistance arteries and arterioles is the main contributor to vascular resistance and, through the arteries' ability actively to change their diameter, an important regulator of local tissue perfusion. However, the passive and active mechanical properties of these vessels have generally been characterised only in terms of gross changes in vessel radius or wall thickness/area in response to changes in transmural pressure or smooth muscle tone. This scale of characterisation is inadequate to understand processes such as the transmission of mechanical signals between blood and vascular cells and the functional significance of the structural and cellular changes that occur with age and in many diseases.

The mechanical properties of large blood vessels are largely passive and the relationship between their non-linear stress-strain behaviour and the extensive networks of compliant elastic fibres and much more rigid collagen fibres has been revealed over many years (13, 55). In small blood vessels smooth muscle cells make an active contribution to vascular mechanics and the ways in which smooth muscle tone is determined both by chemical signals and by the complex patterns of mechanical forces, including fluid- and solid-shear stress and pressure have been extensively documented (21, 35). However, our understanding of small vessel biomechanics is otherwise still somewhat limited. Small artery mechanics are generally characterised by a singular "stiffness", a parameter which is used, for example, to characterise vessel remodelling in disease (38, 39, 56). Stiffness is generally determined from microscopic measurements of the apparent internal and external diameters of a vessel mounted on a pressure myograph (18, 30) and analysis is based upon the assumption that the blood vessel is homogeneous in its composition and mechanical properties. The vast differences in the mechanical properties of different regions of blood vessels, which has been demonstrated in large arteries by, for example, the work of Holzapfel (24, 25), shows that whole-vessel calculations of quantities such as wall stress and radial strain do not reflect the intramural mechanical environment. There is an urgent need to extend micro-scale analysis to the small vessels.

The manner in which an elastic fibre network allows large-scale distention, which is arrested by a network of collagen fibres that prevent damaging over-extension has been observed in many tissues (16, 40). In large arteries significant progress has been made in quantifying the orientation of fibrous networks (44), the mechanical relationship between collagen and elastic fibres (10, 15, 50), and the mechanical effect of vascular tone (54). To date there has been no similar characterisation of small arteries. The radial distension of small arteries under increasing transmural pressure in the absence of myogenic responses has been described by multi-parameter "hook-on" models (3), and, more recently serial element models (52). These are essentially two-phase linear or hyper-elastic models that account for strain-dependent recruitment of collagen fibres, and urgently require support from microstructural observations.

In order to test and extend models to a level where they can be used to evaluate the functional significance of changes in structure and composition it is necessary not only to visualise the three dimensional structure of the intact vessel, but also continuously to observe the changes that occur during pressurisation or alterations in muscle tone. Only against this background can the functional significance of changes that occur with age (12), lifestyle (18), disease (34), and body location (11) be fully understood. These objectives can be realised using nonlinear microscopy (NLM), a technique that recently has been reviewed in the context of vascular disease, (32) and employed in the characterisation of static resistance arteries (6).

In the present investigation, unfixed human small resistance arteries mounted in a perfusion myograph were repeatedly imaged as transmural pressure was increased. Two photon

fluorescence (TPF) revealed elastic fibres and other, intracellular, auto-fluorescent proteins, while second harmonic generation (SHG) revealed fibrous collagen. Three-dimensional reconstructions of the co-registered TPF and SHG images revealed separate layers in the extracellular matrix of the vessel wall, while nuclear staining using 4',6-Diamidino-2-Phenylindole dilactate (DAPI) provided information about the distribution of cells in relation to these layers. A simple, two-layer analytical model of the vessel wall was constructed using the images to determine the distribution of strain, and thereby to infer the variation in stiffness and circumferential stress across the vessel wall. The mechanical interplay between the highly extensible elastic fibre network and the inextensible collagen network is analysed by calculating the distributions of orientation, and changes associated with increased transmural pressure.

Materials and Methods

The study was performed on resistance arteries from healthy human volunteers recruited from the Exeter Ten Thousand (EXTEND) cohort. Following the administration of a local anaesthetic a subcutaneous abdominal adipose tissue biopsy was removed by scalpel incision at 10 cm laterally to the right of the umbilicus and immediately transported to the microscopy laboratory. Fully informed written consent was obtained in accordance with the Declaration of Helsinki. Ethics approval was granted by the NRES Committee South West – Exeter (Ref no: 11/SW/0199).

During transport and dissection, the tissue sample was immersed in 3-[*N*-morpholino]propane sulfonic acid (MOPS) buffer (at 4°C) containing (in mmol/L): 145 NaCl, 4.7 KCl, 2.0 $CaCl_2(2H_2O)$ 1.17 $MgSO_4(7H_2O)$, 2.0 MOPS, 1.2 $NaH_2PO_4(H_2O)$, 5.0 glucose, 2.0 pyruvate, 0.02 EDTA, and 2.75 NaOH adjusted to pH 7.40±0.02. Small resistance arteries were visualised under a dissection microscope and adipocytes and excess connective tissue were removed leaving the adventitia intact. Segments approximately 3-5 mm in length, with an outer diameter of 200-400 μm and without visible side-branches were deemed suitable for cannulation. Arteries were carefully transferred to a custom-made myograph bath containing chilled MOPS buffer (4 ^{o}C).

The vessel preparation protocol was adapted from a previous study (28). The dissected resistance arteries were cannulated with glass capillary tubes pulled to a diameter of approximately 20 μm attached to the myograph, and secured with 11-0 gauge suture (Ethicon). During the mounting process the vessels were perfused to remove blood from the lumen, taking care to prevent introducing bubbles and damage to the endothelium. The capillary tubes were then moved apart until the vessels were straight but not stretched, before being placed on the microscope stage. The myograph bath was maintained at 37°C using a pump and heat exchanger. Transmural pressure was controlled using medium-filled pressure reservoirs connected to the capillary tubes, which were maintained at a minimum transmural pressure of 3 mmHg to prevent vessel collapse. Images were acquired at 3, 10, 20, 30 mm and 50 mm Hg (the physiological pressure range in these vessels is believed to be 40-90 mmHg, as discussed below). Vessels were allowed to equilibrate for 15 minutes following a pressure increment before imaging. The myograph included the facility to adjust longitudinal strain if vessels bent following changes in pressure, although it was not needed.

The nonlinear microscopy system comprised a modified confocal laser-scanning microscope (FluoView IX71 and F300, Olympus) and Ti:sapphire laser (816 nm, Mira 900-D, Coherent) pumped by a 532 nm solid state laser (Verdi V10, Coherent) with a repetition rate of 76 MHz and a pulse width of 100 fs. TPF and SHG signals were separated from the laser fundamental using a long pass dichroic mirror (670dcxr, Chroma Technologies, part 7 in 2.5b) before being

separated from one another by a second long pass dichroic mirror (Di02-R405, Semrock). The TPF signal was passed through two band-pass filters (F70-500-3-PFU and CG-BG-39, CVI Melles Griot) centred at 500 nm with FWHM of 70 nm, and the SHG signal was passed through two band pass filters (FF01-405, Semrock and CG-BG-39, CVI Melles Griot) centred at 405 nm with FWHM of 10 nm. This matches closely the spectral peak of TPF for elastin (36) and that of SHG for collagen (31). The signal was focused into a photomultiplier tube (Hamamatsu R3896). Olympus UPlanSApo 20× 0.4 NA and 60× 1 NA water immersion objectives were used to obtain 500 nm resolution *en-face* and sagittal images to a depth of up to 200 μm. Each 512×512 pixel image took 22 seconds to capture, and was incremented in *z* by 1 μm. A typical 135 μm stack therefore took approximately 50 minutes to complete. After the 30 mmHg SHG/TPF imaging protocol, for vessels that were not chosen for the incremental layer stress study DAPI nuclear stain (Sigma) was mixed into the bathing solution at a final concentration of 500 nM. An image stack was then taken to reveal the distribution of cell nuclei.

Image stacks were converted into 3D images using the Volume Viewer plugin for Fiji (42). Vessel radii and wall layer thicknesses were calculated by fitting circles to the inner and outer vessel boundaries, as well as the interface between the media and adventitia, which was demarcated by a step in SHG signal. Where vessels had irregular shapes, circles were fitted such that circle area matched that of the region of interest. Measurements were taken for at least 5 longitudinal points per vessel, and verified by plotting signal intensity profiles through the wall. The OrientationJ Distribution plugin for Fiji (37) was used to quantify the orientation of the intimal and adventitial elastic fibre networks, and the collagen network.

The wall strains associated with increasing luminal pressure were modelled analytically using linear thick walled cylinder theory (see (53) for a full derivation). Briefly, assuming negligible torsion and axial strain, the displacement field $u = u_r$ for each layer is described by the continuity equation:

$$\frac{d^2u_r}{dr^2} + \frac{1}{r}\frac{du_r}{dr} - \frac{u_r}{r^2} = 0 \quad (1)$$

with the general solution:

$$u_r = \frac{C_{r1}}{r} + C_{r2}r \quad (2)$$

Assuming radial displacement and stresses are continuous across the layer interface and that the pressure outside the vessel is zero, the values of C_{r1} and C_{r2} can be calculated for each layer from the inner radius r_i, the outer radius r_o, the elastic modulus E, the Poisson's ratio ν and the lumen pressure p. Radial deformations were calculated for given E_i, ν_i, E_o, ν_o (subscripts *i* and *o* refer to inner and outer layer, respectively) and a brute-force minimisation algorithm was written to find the material parameters that optimally map vessel geometry at 3 mmHg transmural pressure to that at 30 mmHg. The objective of the algorithm was to minimise the sum of the squares of the errors in the layer boundary positions. The same model was used to determine material parameters for a homogeneous model assuming the vessels to be a single layer.

Standard hoop stress, σ, referred to in myography as "media stress" (27), in a homogeneous tube is defined as:

$$\sigma = \frac{pr_i}{r_o^2 - r_i^2} + \frac{pr_i^2 r_o^2}{r^2\left(r_o^2 - r_i^2\right)} \quad (3)$$

.

Circumferential stress in the two layer model is defined as

$$\sigma_{\theta\theta} = E\frac{(1-2\nu)C_{r1} + r^2 C_{r2}}{r^2(1-2\nu)(1+\nu)} \quad (4)$$

and, to act as a true comparator to hoop stress, the effect of circumferential expansion pressure due to radial strain is ignored.

Unless otherwise stated, data are presented as mean ± SEM. Statistical significance was calculated using t-tests with the null hypothesis rejected at the 5% significance level. The Spearman correlation was used to determine whether changes in features on orientation plots correlated with changes in mechanical properties.

Results

Vessels were obtained from 12 healthy subjects. Table 1 summarises the measurements taken from each volunteer/sample. It was possible to discern some commonly occurring structural features and responses to increasing pressures, which we describe first. We then describe marked differences that were observed in some vessels.

Vessel morphology

TPF imaging showed two morphologically distinct networks of elastic fibres, one which formed an internal elastic layer (IEL) and another in the adventitia, whose density varied between subjects. The IEL contained longitudinally-aligned fibres up to 5 μm in diameter, braced by thinner fibres <1-2 μm in diameter. Adventitial elastic fibres were generally less than 1 μm in diameter, although fibres up to 3 μm in diameter were sometimes found, particularly in vessels with denser adventitial elastic fibre networks. SHG revealed a network of collagen fibres forming bundles between 3 and 35 μm in diameter in the adventitia. No fibrous collagen was found in the media or intima of any subjects.

Figures 1 and 2 show co-registered TPF (green, predominantly elastic fibres) and SHG (blue, collagen) images of a typical vessel obtained from subject 11 at transmural pressures of 3 and 30 mmHg, respectively. Supplemental videos 1A-D show progressive sections through the artery in each of the imaging modalities.

At the lower pressure the average internal diameter was 138 μm and the average external diameter 262 μm, giving an average wall thickness of 62 μm. Figure 1A shows a longitudinal section through the adventitia at low pressure, which comprises discrete bundles of wavy or helically wound collagen, which are inter-woven and punctuated by a sparse network of adventitial elastic fibres. Both components are predominantly aligned longitudinally. The collagen bundles have a helical/wavy periodicity of between 20 and 50 μm, scaling with bundle diameter. Elastic fibres run between and through the collagen helices and pass continuously across the adventitia:media boundary. Figure 1B shows a longitudinal section through the vessel wall with the adventitia and media at the sides, and the IEL in the middle. Longitudinal fibres of the IEL appear closely packed and occasionally overlap, with bracing fibres spaced at regular intervals of 15-20 μm. The small spots of TPF in the media are believed to be

fluorescent cellular proteins. Figures 1C and 1D show radial sections, and a 3D perspective view of the vessel, respectively. These views reveal the fibrous adventitia, the dark, predominantly cellular media and the highly fluorescent IEL of the intima. The adventitia is 25 μm thick while the intima and media combined form a layer 37 μm thick.

Raising the transmural pressure to 30 mmHg causes the internal and external diameters to increase to 172 μm and 286 μm, respectively. The corresponding average circumferential strains at the inner and outer edges of the vessel are 25% and 9%, respectively, while the vessel wall volumetric strain is 5%. The adventitia, pictured in Figure 2A, exhibits slightly straighter collagen fibre bundles, oriented less predominantly in the longitudinal direction. The IEL, pictured in Figure 2B, accommodates the high lumen strain by increasing the gaps between the longitudinal fibres, with the thinner bracing fibres forming a honeycomb structure in places. This pattern of deformation results in a very heterogeneous distribution of local strains, peaking at over 200% in the region between fibres. The section and 3D views in Figures 2C and 2D show that the elastic inner wall assumes a more uniform cylindrical contour as pressure is increased. The radial thickness of the intima and media is reduced by 4 μm to 33 μm while the adventitia reduced by 1 μm to 24 μm. The corresponding radial and volumetric strains for the media are -11% and 4%, and for the adventitia are -4% and 19%.

Figure 3 shows sections through a vessel obtained from subject 9, 332 μm in outer diameter at 30 mmHg transmural pressure, stained with DAPI for cell nucleus visualisation. Panels A, B, C, D are taken at positions of 10 μm, 47 μm, 68 μm and 86 μm, respectively from the outer edge. Adventitial cells (presumed to be fibroblasts) exhibit no preferential orientation, medial vascular smooth muscle cells (VSMCs) are predominantly aligned circumferentially, and intimal endothelial cells are aligned longitudinally. The positions of endothelial cell nuclei bear no spatial relationship relative to individual fibres in the IEL: nuclei are observed in positions adjacent to elastic fibre intersections, as well as mid-way between. The radial distance between endothelial cell nuclei and the IEL is below the resolution of the microscope, meaning the basement membrane, which contains Type IV collagen and does not generate SHG, must occupy a region less than 1 μm thick. The VSMC nuclei have a high slenderness ratio and are aligned circumferentially, with a slight helical bias. They vary in length between 17 μm and 44 μm, with an average of 31 μm. The muscle cell nuclei occupy 20±1% of the medial volume in all vessels. The innermost layer of VSMCs press against the IEL. The outer VSMC nuclei and adventitial collagen border, and in some cases slightly interpenetrate one another.

Individual variations

5 of the 12 vessels were irregular in wall thickness around their circumference, being up to one third thinner over 2.5% to 6% of the circumference due to a dip in the outer radius as illustrated in Figure 4A (arrow). The circumferential position of the thin region spiralled around the vessel along its length with an axial periodicity of between 400 μm and 968 μm.

3 of the 12 vessels showed significantly greater amounts of fibrous protein in the adventitia, such as the example shown in longitudinal section in Figure 4B and supplemental videos 2A-D. In these vessels the adventitia comprised over half the thickness of the vessel wall, compared to an overall average of 40%**.** Adventitial elastic fibres were thicker and formed a continuous layer around the outside of the adventitia up to three fibres thick, while the collagen was arranged in thicker, more tightly woven bundles. This morphology was distinct from that of the adipose tissue in which the vessel had been embedded. At 30 mmHg transmural pressure the innermost collagen was arranged in straight bundles at ±45° to the longitudinal direction.

Two vessels underwent myogenic contraction during observation and in this case the relatively uniform cylindrical morphology of the IEL became corrugated as shown in Figure 4C. These corrugations were up to 5 μm deep and 100 μm long.

Fine elastic fibres less than a micron thick were observed penetrating radially into the media from the adventitia before aligning circumferentially between VSMCs (Figure 4D). These fibres are particularly clear in the TPF supplemental videos.

Wall mechanics

7 vessels were analysed using the analytical models. Exclusion criteria included unclear layer boundaries in the images due to scattering and myogenic events. The geometry and fitted mechanical parameters for the one and two layer models are summarised in Table 2, and shown graphically in Figure 5A. In the two layer model the radial strains in each layer are not significantly different but the corresponding elastic moduli are (E_m = 18.2 ± 5.4 kPa vs E_a = 182 ± 60 kPa, $p<0.05$). The range in volumetric strain of both layers (Figure 5B) was considerable, and for the number of vessels examined no significant difference between the layers was established.

An analysis of peak wall stress associated with increasing lumen pressure (referred to as 'media stress' in the myography literature) for the vessel depicted in Figures 1 and 2 is shown in Figure 5C. At pressures of 30 mmHg and below, the stress is relatively uniform across the vessel, but at 50 mmHg the adventitia experiences more than twice the stress in the media. Over the whole group of vessels the pressure at which the adventitia takes up the majority of the wall stress decreased as the lumen diameter increased. The ratio of adventitial circumferential stress ($\sigma_{\theta a}$) to media circumferential stress ($\sigma_{\theta m}$) at 30 mmHg is plotted in Figure 5D.

The single layer model, which is widely used to estimate wall stiffness, yielded stiffness values generally between those of the adventitia and media in the two layer model (E_h = 67.9 ± 12.9 kPa). This value was significantly different from the media stiffness in the two layer model ($p<0.01$). Circumferential stress derived from the single layer model was generally greater than that calculated directly for the adventitia in the layered model for smaller vessels, but smaller for the larger vessels, and was always many times greater than that in the media. The discrepancies between the two models increased with lumen diameter.

Fibre orientation

The average spreads of orientation in the fibrous protein networks are shown in Figure 6, where 90° represents longitudinal alignment and 0°/180° represent circumferential. In all vessels the distributions became more isotropic with distension. The preferred orientation of adventitial elastic fibres moved in the same direction in all samples, suggesting recruitment into a left-handed helical arrangement. Measurements of full width half maximum (FWHM – a measure of orientation dispersion), peak orientation and maximum:minimum orientation ratio (a measure of isotropy) were made for each sample at 3 mmHg and 30 mmHg transmural pressure, and are shown in Table 3.

There were Spearman correlations ($r_s < 0.05$) between adventitial elastic fibre FWHM and adventitia stiffness, adventitial elastic fibre FWHM and adventitia strain, and IEL FWHM and media strain. The ratio of minimum to maximum collagen orientation correlated weakly with both adventitia stiffness and strain ($r_s < 0.1$).

Discussion

The microstructure of human resistance arteries, and changes associated with transmural pressure, have been visualised using NLM and analysed from a morphological and mechanical perspective. The structure of the small arteries employed in these studies using nonlinear microscopy was consistent with that observed in fixed human pulmonary resistance arteries (6), with the exception that in this study no fibrous collagen was observed in the media. The structure of the two fibrous networks in the adventitia was similar to that seen in both large (10, 50) and small (6) arteries. It was notable that none of the vessels contained the fenestrated sheets of elastin reported in the intima of resistance arteries in other studies (11).

A focus of the present research was the structural changes accompanying increases in luminal pressure, which differed in each of the fibrous protein networks. In the IEL the fibres were predominantly axially aligned at low pressure, but at higher pressure spread apart to reveal gaps bridged by regularly spaced bracing fibres, which appear on the orientation plot as an emerging peak around 0°. This honeycomb-like structure has been visualised at much higher pressures (6), and its mechanical properties analysed in large arteries (10).

Collagen fibres were found in this study to straighten with increasing pressure and become more isotropic in orientation, which is a common observation in arteries (10, 15, 50). In some vessels there was radius-dependent recruitment of collagen (see supplemental video 2D), as has been previously noted in larger arteries (10) with the same pattern of orientation (24). This behaviour may be responsible for the reduced distensibility known to be associated with increased transmural pressure (47).

The adventitial elastic fibres exhibited the most unexpected response to transmural pressure in that the preferential orientation shifted to a left-handed helical state. The reorientation was less than that of the neighbouring collagen network, demonstrating the complexity of the strain fields at the fibrillar level. We suggest that the fine circumferential elastic fibres in the media act as “anchoring points” and possess a role in restoring the geometry of the networks after cellular relaxation or in distributing interfacial stresses arising from the different mechanical properties of media and adventitia. Elastin-deficient mice have twisted and tortuous aortae (9), so it is also possible that adventitial elastic fibres mediate torsion in resistance arteries.

The very large local strains between elastic fibres of the IEL raise questions concerning the coupling of VSMCs with matrix fibres. It is known, for example that displacement by as little as 30 nm of a focal adhesion in a VSMC can provoke a myogenic response (46) and it may be that it is possible that the bracing fibres, which experience far less circumferential strain, act as strain-protected anchoring sites for VSMCs. There are similar questions concerning the attachment of the endothelial cells to the underlying matrix and a particular issue here is the corrugations that were produced in the IEL during myogenic contraction. The basement membrane cannot be imaged directly (type IV collagen does not produce SHG), but it must be less than 1 μm in thickness as no gap between endothelial cell nuclei and elastic fibres could be resolved. Furthermore, endothelial cell nuclei were found both in the grooves of the corrugations and exposed on the ridges, indicating that the cells followed the underlying contours, suggesting an intimate coupling of IEL to basement membrane. Given the local strains between elastic fibres of the IEL were found to exceed 200%, this further suggests that the Type IV collagen network that comprises the skeleton of basement membrane structure routinely experiences strains of a similar magnitude. Whist Type IV collagen is believed to be quite stiff, network arrangements such as honeycomb or chicken wire have been proposed (51, 57), which could

have the requisite compliance. Whether the transient development of intimal corrugations has implications for the structure of the haemodynamic boundary layer and fluid mechanical forces on the endothelium remains to be explored. However, the effects of substrate strain on endothelial cells have been extensively investigated (7), demonstrating that they respond to strains of the order of 10% (49). Circumferential strains of this magnitude were measured locally in all vessels during each 10 mmHg increase in transmural pressure. It therefore is probable that changes in the basement membrane, which are characteristic of diseases such as diabetes (1), and endothelial cell integrin expression may affect endothelial cell mechanotransduction (45), as well as the mechanical properties of the intima.

The medial volume is largely occupied by smooth muscle cells. At intermediate pressure (30 mmHg), cell nuclei occupied 20±1% of the medial volume and since in VSMCs the nuclei comprise 20% of the total cell volume (48) the media is almost completely cellular. This is consistent with the nearly complete absence of fibrillar proteins, and would maximise the ability of the vessel to adjust its radius through changes in cellular tone. This ability is further enhanced by the relative stiffness of the adventitia, which forms a stiff boundary for the muscle cells to act against. When the cells are in a passive state the media deforms less than the adventitia under luminal pressure increase, yet has one tenth the stiffness: luminal pressure is balanced by the circumferential stress in the adventitia, whilst medial compliance allows changes in muscle tone to modulate the inner radius of the vessel. Changes in vascular tone, which have been shown to affect incremental distensibility (47) are likely to lead to a redistribution in circumferential stress and this will be a target of continuing work.

In most vessels the volume of the adventitia fell as transmural pressure increased, suggesting that as the constraint imposed by the adventitia becomes significant (52) the inner-lying matrix is compressed, as observed in tensile testing (4). These volume changes in the extracellular matrix arise from the exudation of interstitial fluid over the timescale of minutes. This movement of fluid is likely to lead to changes in the interstitial ionic concentration if, as is likely, the matrix has an appreciable fixed charge density. In other tissues such as cartilage these changes are known to influence cellular metabolism (20). Such poroelastic behaviour also presents a challenge for the development of models of microvascular wall mechanics incorporating poroelasticity such as those proposed for large vessels (29) and cartilage (33).

In the vessels used in this study the morphology and composition of the adventitia varied more than that of the intima and media and several biopsies contained vessels with different adventitial morphologies. However, in this small study of subjects of healthy weight we could establish no correlations between fibrous protein morphology or quantity and variables such as vessel diameter (which varied by a factor of two) or clinical indices such as BMI or blood pressure. Samples from older volunteers may have been stiffened through normal ageing or fibrosis or other undetected pathologies (19). However, a recent study on the mechanics of the adipose tissue (2) from which the vessels were isolated revealed it to be mechanically very heterogeneous and the adventitial variability may reflect the differing requirements of its role in coupling the vessel to the surrounding tissue. Constrained mixture modelling has been successful in quantifying the mechanical effect of changes in individual fibrous protein networks (8) and similar modelling for microvessels is needed to understand the extent of mechanical variation between the different microvessel morphologies shown in this study.

Implications for the understanding of small vessel mechanics and pathology

Our data could provide the basis of structurally-based numerical models of microvessel mechanics. In the meantime it is of interest to discuss them in the context of established

models, though our work exposes certain limitations. The observation that the media experiences much less circumferential stress than the adventitia cannot be accommodated in a homogeneous model, and as noted above the changes in medial volume during pressurisation suggest the need for a poroelastic model. The mechanical model used in this study highlights misconceptions arising from the use of simple homogeneous models, but itself has further limitations. It does not take into consideration the effect of internal stress, which is known to be significant in large arteries (5, 15) or the anisotropy, which has been shown morphologically in this work to be significant. There has been extensive work in theoretical modelling of these two factors in large arteries (14, 17, 23, 58), and to fully understand the mechanical environment of the resistance artery, similar work is needed.

A key target of modelling is to understand the changes associated with hypertension, which is reported to cause vessel walls to become less stiff (26). This behaviour has been analysed in terms of Laplace's equation for cylinder stress, which states that circumferential wall stress increases linearly with lumen radius (41). This equation only applies for a homogenous, thin-walled cylinder. In a thick-walled cylinder such as a resistance artery, if homogeneity is assumed the distribution of wall stress is inversely proportional to r^2, placing the peak stress in the cellular intima and media. Decreasing the lumen diameter and increasing the wall:lumen ratio reduces the total wall stress, as is considered beneficial, but a greater proportion of the stress is placed on the media, which may be less advantageous. Collagen fibre recruitment has been shown in this study to lead to circumferential stiffening of the adventitia, which causes the vessel wall to thin under increased transmural pressure as the inner layers press up against it. This adventitial stiffening also transfers circumferential stress from the inside of the vessel to the outside. This stiffening effect is commonly misinterpreted as a drop in wall stiffness, due to the common practise of quantifying arterial wall mechanics using changes in internal and external diameter. A micromechanical study of diseased vessels is urgently needed to elucidate how the micromechanical environment is changed by pathological vascular remodelling.

Limitations

The statistical power of our analysis was limited by the small number of samples, even though subjects were recruited over a prolonged period. A primary factor was that of the abdominal subcutaneous fat biopsies only 70% yielded a suitable resistance artery, and of the 12 arteries obtained, only 7 were suitable for mechanical analysis. It may be that other sampling sites would be more productive. Articles citing buttock biopsies as the source of subcutaneous tissue do not report such problems (43). Because of the small sample numbers we were unable systematically to vary smooth muscle tone, which is known to make a variable contribution to mechanics (22). Instead the vessels were imaged at what we presumed to be basal tone giving pressure-diameter curves in the middle of their expected range (47).

Another mechanical parameter which was poorly controlled was longitudinal tension. What longitudinal tensions a microvessel might experience in adipose tissue in vivo is an interesting question, and in the absence of an answer we mounted vessels at the minimal straightened length. Changing luminal pressure altered longitudinal strain and by tracking fiducial markers on the adventitial surface of a single vessel we found this to be, on average, 2.9% over the pressure range employed. This is small compared to the radial distension, but could be examined more rigorously using digital image correlation techniques and it may be important to incorporate such information in finite element models. Another uncertainty was the physiological pressures in the microvessels. It may have been higher than the range 3-50 mmHg we employed, but this was chosen as being the one over which most structural changes occurred: extending the range would have meant unacceptable extension of the imaging time.

Conclusion

The three fibrous protein networks in human subcutaneous resistance arteries have been imaged at incremental transmural pressures in three dimensions at high resolution, and they have been found each to possess unique mechanical characteristics. A two-layer mechanical model predicts that the adventitia is significantly stiffer than the media at pressures sufficient to recruit its extensive network of collagen, and therefore bears the vast majority of the circumferential stress in the passive state. Orientation analysis provides a first step towards understanding the anisotropic nature of the vessel wall. Our findings have implications for the understanding of small artery biomechanics and related pathologies.

Grants

The research was funded by the British Heart Foundation grant no PG/11/17/28788 and supported by the National Institute for Health Research (NIHR) Exeter Clinical Research Facility. The views expressed are those of the author(s) and not necessarily those of the NHS, the NIHR or the Department of Health.

Disclosures

None declared.

References

1. **Ali L**, **Bradley DA**, **Ellis RE**, **Green E**, **Grossmann JG**, **Winlove CP**. The structure and organisation of type-IV collagen in normal and glycated basement membrane. *Radiat Phys Chem* 71: 953–956, 2004.

2. **Alkhouli N**, **Mansfield J**, **Green E**, **Bell J**, **Knight B**, **Liversedge N**, **Tham JC**, **Welbourn R**, **Shore AC**, **Kos K**, **Winlove CP**. The mechanical properties of human adipose tissues and their relationships to the structure and composition of the extracellular matrix. *Am J Physiol Endocrinol Metab* 305: E1427–35, 2013.

3. **Bank AJ**, **Wang H**, **Holte JE**, **Mullen K**, **Shammas R**, **Kubo SH**. Contribution of Collagen, Elastin, and Smooth Muscle to In Vivo Human Brachial Artery Wall Stress and Elastic Modulus. *Circ* 94 : 3263–3270, 1996.

4. **Bell JS**, **Christmas J**, **Mansfield JC**, **Everson RM**, **Winlove CP**. Micromechanical response of articular cartilage to tensile load measured using nonlinear microscopy. *Acta Biomater* 10: 2574–2581, 2014.

5. **Berry JL**, **Rachev A**, **Moore JE**, **Meister J-J**. Analysis of the effects of a non-circular two layer stress-free state on arterial wall stresses. In: *Engineering in Medicine and Biology Society, 1992 14th Annual International Conference of the IEEE*, 1992.

6. **Bloksgaard M**, **Leurgans TM**, **Nissen I**, **Jensen PS**, **Hansen ML**, **Brewer JR**, **Bagatolli LA**, **Marcussen N**, **Irmukhamedov A**, **Rasmussen LM**. Elastin organization in pig and cardiovascular disease patients' pericardial resistance arteries. *J Vasc Res* 52: 1–11,

2015.

7. **Califano JP**, **Reinhart-King CA**. Exogenous and endogenous force regulation of endothelial cell behavior. *J Biomech* 43: 79–86, 2010.

8. **Cardamone L**, **Valentin A**, **Eberth JF**, **Humphrey JD**. Modelling carotid artery adaptations to dynamic alterations in pressure and flow over the cardiac cycle. *Math Med Biol* 27: 343–371, 2010.

9. **Carta L**, **Wagenseil JE**, **Knutsen RH**, **Mariko B**, **Faury G**, **Davis EC**, **Starcher B**, **Mecham RP**, **Ramirez F**. Discrete contributions of elastic fiber components to arterial development and mechanical compliance. *Arterioscler Thromb Vasc Biol* 29: 2083–2089, 2009.

10. **Chow M-J**, **Turcotte R**, **Lin CP**, **Zhang Y**. Arterial extracellular matrix: a mechanobiological study of the contributions and interactions of elastin and collagen. *Biophys J* 106: 2684–2692, 2014.

11. **Clifford PS**, **Ella SR**, **Stupica AJ**, **Nourian Z**, **Li M**, **Martinez-Lemus L a**, **Dora K a**, **Yang Y**, **Davis MJ**, **Pohl U**, **Meininger G a**, **Hill M a**. Spatial distribution and mechanical function of elastin in resistance arteries: a role in bearing longitudinal stress. *Arterioscler Thromb Vasc Biol* 31: 2889–96, 2011.

12. **Cox R**. Age-related changes in arterial wall mechanics and composition of NIA Fischer rats. *Mech Ageing Dev* 23: 21–36, 1983.

13. **Dobrin PB**. Vascular Mechanics. In: *Handbook of Physiology*, edited by Shepherd JT, Abboud FM. Bethesda, MD: 1983.

14. **Driessen NJB**, **Wilson W**, **Bouten CVC**, **Baaijens FPT**. A computational model for collagen fibre remodelling in the arterial wall. *J Theor Biol* 226: 53–64, 2004.

15. **Fata B**, **Carruthers CA**, **Gibson G**, **Watkins SC**, **Gottlieb D**, **Mayer JE**, **Sacks MS**. Regional structural and biomechanical alterations of the ovine main pulmonary artery during postnatal growth. *J Biomech Eng* 135: 21022, 2013.

16. **Fung YC**. *Biomechanics Mechanical Properties of Living Tissues*. Springer-Verlag New York Inc., 1981.

17. **Gasser TC**, **Ogden RW**, **Holzapfel GA**. Hyperelastic modelling of arterial layers with distributed collagen fibre orientations. *J R Soc interface* 3: 15–35, 2006.

18. **Grassi G**, **Seravalle G**, **Scopelliti F**, **Dell'Oro R**, **Fattori L**, **Quarti-Trevano F**, **Brambilla G**, **Schiffrin EL**, **Mancia G**. Structural and functional alterations of subcutaneous small resistance arteries in severe human obesity. *Obesity* 18: 92–8, 2010.

19. **Greenwald SE**. Ageing of the conduit arteries. *J Pathol* 211: 157–172, 2007.

20. **Grodzinsky AJ**, **Levenston ME**, **Jin M**, **Frank EH**. Cartilage Tissue Remodelling in Response to Mechanical Forces. *Annu Rev Biomed Eng* 2: 691–713, 2000.

21. **Hahn C**, **Schwartz MA**. Mechanotransduction in vascular physiology and atherogenesis. *Nat Rev Mol Cell Biol* 10: 53–62, 2009.

22. **Hanna MA**, **Taylor CR**, **Chen B**, **La H-S**, **Maraj JJ**, **Kilar CR**, **Behnke BJ**, **Delp MD**, **Muller-Delp JM**. Structural remodeling of coronary resistance arteries: effects of age and exercise training. *J Appl Physiol* 117: 616–623, 2014.

23. **Hariton I**, **Gasser TC**, **Holzapfel GA**, **others**. Stress-driven collagen fiber remodeling in arterial walls. *Biomech Model Mechanobiol* 6: 163–175, 2007.

24. **Holzapfel G**, **Gasser T**, **Ogden R**. A New Constitutive Framework for Arterial Wall Mechanics and a Comparative Study of Material Models. *J Elast Phys Sci solids* 61: 1–48, 2000.

25. **Holzapfel GA**, **Gasser TC**, **Stadler M**. A structural model for the viscoelastic behavior of arterial walls: Continuum formulation and finite element analysis. *Eur J Mech - A/Solids* 21: 441–463, 2002.

26. **Intengan HD**, **Deng LY**, **Li JS**, **Schiffrin EL**. Mechanics and Composition of Human Subcutaneous Resistance Arteries in Essential Hypertension. *Hypertension* 33: 569–574, 1999.

27. **Intengan HD**, **Schiffrin EL**. Structure and Mechanical Properties of Resistance Arteries in Hypertension : Role of Adhesion Molecules and Extracellular Matrix Determinants. *Hypertension* 36: 312–318, 2000.

28. **James MA**, **Tullett J**, **Hemsley AG**, **Shore AC**. Effects of Aging and Hypertension on the Microcirculation. *Hypertension* 47: 968-974, 2006.

29. **Kenyon DE**. Mathematical-Model of Water Flux through Aortic Tissue. *Bull Math Biol* 41: 79–90, 1979.

30. **Laurant P**, **Touyz RM**, **Schiffrin EL**. Effect of Pressurization on Mechanical Properties of Mesenteric Small Arteries from Spontaneously Hypertensive Rats. *J Vasc Res* 34: 117–125, 1997.

31. **Mansfield JC**, **Winlove CP**, **Knapp K**, **Matcher SJ**. Imaging articular cartilage using second harmonic generation microscopy. In: *Biomedical Optics 2006*, International Society for Optics and Photonics, 2006.

32. **Megens RTA**, **Bianchini M**, **Schmitt MMN**, **Weber C**. Optical Imaging Innovations for Atherosclerosis Research Multiphoton Microscopy and Optical Nanoscopy. *Arterioscler Thromb Vasc Biol* 35: 1339–1346, 2015.

33. **Mow VC**, **Holmes MH**, **Lai WM**. Fluid Transport and Mechanical Properties of Articular Cartilage: A Review. *J Biomech* 17: 377–394, 1984.

34. **Mulvany MJ**. Small artery remodelling in hypertension. *Basic Clin Pharmacol Toxicol* 110: 49–55, 2012.

35. **Nelson MT**, **Patlak JB**, **Worley JF**, **Standen NB**. Calcium channels, potassium channels, and voltage dependence of arterial smooth muscle tone. *Am J Physiol Cell Physiol* 259: C3–C18, 1990.

36. **Palero JA**, **de Bruijn HS**, **van den Heuvel A V**, **Sterenborg HJCM**, **Gerritsen HC**. Spectrally resolved multiphoton imaging of in vivo and excised mouse skin tissues. *Biophys J* 93: 992–1007, 2007.

37. **Rezakhaniha R**, **Agianniotis A**, **Schrauwen JTC**, **Griffa A**, **Sage D**, **Bouten CVC**, **de Vosse FN**, **Unser M**, **Stergiopulos N**. Experimental investigation of collagen waviness and orientation in the arterial adventitia using confocal laser scanning microscopy. *Biomech Model Mechanobiol* 11: 461–473, 2012.

38. **Rizzoni D**, **Porteri E**, **Guelfi D**, **Muiesan ML**, **Valentini U**, **Cimino a.**, **Girelli a.**, **Rodella L**, **Bianchi R**, **Sleiman I**, **Rosei E a.** Structural Alterations in Subcutaneous Small Arteries of Normotensive and Hypertensive Patients With Non-Insulin-Dependent Diabetes Mellitus. *Circulation* 103: 1238–1244, 2001.

39. **Rizzoni D**, **Rosei EA**. Small artery remodeling in diabetes mellitus. *Nutr Metab Cardiovasc Dis* 19: 587–92, 2009.

40. **Roach MR**, **Burton AC**. The reason for the shape of the distensibility curves of arteries. *Can J Biochem Physiol* 35: 681–690, 1957.

41. **Savoia C**, **Schiffrin EL**. Vascular Changes in the Microcirculation: Arterial Remodeling and Capillary Rarefaction. In: *Arterial Disorders,* edited by Berbari A, Mancia G. Springer, 2015.

42. **Schindelin J**, **Arganda-Carreras I**, **Frise E**, **Kaynig V**, **Longair M**, **Pietzsch T**, **Preibisch S**, **Rueden C**, **Saalfeld S**, **Schmid B**, **Tinevez J-Y**, **White DJ**, **Hartenstein V**, **Eliceiri K**, **Tomancak P**, **Cardona A**. Fiji: an open-source platform for biological-image analysis. *Nat Meth* 9: 676–682, 2012.

43. **Schofield I**. Vascular Structural and Functional Changes in Type 2 Diabetes Mellitus: Evidence for the Roles of Abnormal Myogenic Responsiveness and Dyslipidemia. *Circulation* 106: 3037–3043, 2002.

44. **Schriefl AJ**, **Reinisch AJ**, **Sankaran S**, **Pierce DM**, **Holzapfel GA**. Quantitative assessment of collagen fibre orientations from two-dimensional images of soft biological tissues. *J R Soc Interface* 9: 3081–3093, 2012.

45. **Shyy JY-J**. Role of Integrins in Endothelial Mechanosensing of Shear Stress. *Circ Res* 91: 769–775, 2002.

46. **Sun Z**, **Martinez-lemus LA**, **Hill MA**, **Meininger GA**. Extracellular matrix-specific focal adhesions in vascular smooth muscle produce mechanically active adhesion sites. *Am J Physiol Cell Physiol* 295 C268–C278 2008.

47. **Szekeres M ria**, **Nadasy GL**, **Dezsi L**, **Orosz M s**, **Tökés A**, **Monos E**. Segmental

differences in geometric, elastic and contractile characteristics of small intramural coronary arteries of the rat. *J Vasc Res* 35: 332–344, 1998.

48. **Thakar RG**, **Cheng Q**, **Patel S**, **Chu J**, **Nasir M**, **Liepmann D**, **Komvopoulos K**, **Li S**. Cell-Shape Regulation of Smooth Muscle Cell Proliferation. *Biophys J* 96: 3423–3432, 2009.

49. **Thodeti CK**, **Matthews B**, **Ravi A**, **Mammoto A**, **Ghosh K**, **Bracha AL**, **Ingber DE**. TRPV4 channels mediate cyclic strain–induced endothelial cell reorientation through integrin-to-integrin signaling. *Circ Res* 104: 1123–1130, 2009.

50. **Timmins LH**, **Wu Q**, **Yeh AT**, **Moore JE**, **Greenwald SE**. Structural inhomogeneity and fiber orientation in the inner arterial media. *Am J Physiol Circ Physiol* 298: H1537–H1545, 2010.

51. **Timpl R**, **Wiedemann H**, **DELDEN V**, **Furthmayr H**, **KÜHN K**. A network model for the organization of type IV collagen molecules in basement membranes. *Eur J Biochem* 120: 203–211, 1981.

52. **VanBavel E**, **Siersma P**, **Spaan J a E**. Elasticity of passive blood vessels: a new concept. *Am J Physiol Heart Circ Physiol* 285: H1986–2000, 2003.

53. **Vedeld K**, **Sollund HA**, **Hellesland J**. Closed Analytical Expressions for Stress Distributions in Two-Layer Cylinders and Their Application to Offshore Lined and Clad Pipes. *J Offshore Mech Arct Eng* 137: 21702, 2015.

54. **Wagner HP**, **Humphrey JD**. Differential passive and active biaxial mechanical behaviors of muscular and elastic arteries: basilar versus common carotid. *J Biomech Eng* 133: 51009, 2011.

55. **Wolinsky H**, **Glagov S**. A lamellar unit of aortic medial structure and function in mammals. *Circ Res* 20: 99–111, 1967.

56. **Yu G**, **Zou H**, **Prewitt RL**, **Hill MA**. Impaired Arteriolar Mechanotransduction in Experimental Diabetes Mellitus. *J Diabetes Complications* 13: 235–242, 1999.

57. **Yurchenco PD**, **Furthmayr H**. Self-assembly of basement membrane collagen. *Biochemistry* 23: 1839–1850, 1984.

58. **Zulliger MA**, **Fridez P**, **Hayashi K**, **Stergiopulos N**. A strain energy function for arteries accounting for wall composition and structure. *J Biomech* 37: 989–1000, 2004.

Subject and sample summary	
Gender M/F	8/4
BMI	24.9 ± 2.5 (mean ± S.D.)
Age (years)	53.6 ± 9.2 (mean ± S.D.)
Systolic BP (mmHg)	122.8 ± 10.1 (mean ± S.D.)
Diastolic BP (mmHg)	75.4 ± 8.1 (mean ± S.D.)
Inner radius (μm)	117 ± 17 μm
Wall:lumen ratio	0.37 ± 0.07
Adventitia:media ratio	0.82 ± 0.12

Table 1: Statistical summary of the gender, body mass index (BMI), age and blood pressure (BP) of the volunteers in this study, and the dimensions of the resistance arteries obtained from subcutaneous fat biopsies at 30 mmHg transmural pressure (mean ± S.E.M. unless otherwise indicated).

Geometrical and mechanical results				
Layer		Thickness	Average radial strain	Elastic modulus
Media	3 mmHg 30 mmHg	23.8 ± 3.6 μm 17.5 ± 2.5 μm	-24 ± 7%	18.3 ± 5.4 kPa
Adventitia	3 mmHg 30 mmHg	23.0 ± 2.7 μm 14.3 ± 1.2 μm	-33 ± 7%	182 ± 60 kPa
Whole Wall	3 mmHg 30 mmHg	51.1 ± 4.2 μm 37.8 ± 3.0 μm	-24 ± 6%	81.0 ± 12.9 kPa

Table 2. Measured thicknesses of intima and media at low and high transmural pressure and calculated mechanical parameters for the layered and homogeneous models (mean ± S.E.M.).

	AEF 3 mmHg	IEL 3 mmHg	Coll 3 mmHg	AEF 30 mmHg	IEL 30 mmHg	Coll 30 mmHg
Peak Position (deg)	91.3 ± 2.08	88.0 ± 1.1	95.3 ± 4.1	96.6 ± 3.2	89.5 ± 2.0	94.9 ± 4.6
Full width Half max. (deg)	21.8 ± 3.1	15.7 ± 1.9	62.8 ± 10.5	25.5 ± 2.6	29.7 ± 7.3	82.8 ± 14.3
Min:Max ratio (a.u.)	2385 ± 1304	571 ± 446	172 ± 154	2401 ± 2173	205 ± 115	130 ± 121

Table 3. Summary of orientation analysis statistics for the three distinct fibrous networks at two pressure increments (AEF adventitial elastic fibres, IEL internal elastic layer, Coll fibrous collagen, mean ± S.E.M.).

Figure Captions

Figure 1. False colour images of a 138 μm lumen diameter vessel at 3 mmHg transmural pressure, showing SHG (collagen) in blue, and TPF (elastic fibres and cellular fluorescence) in green. Red labels: A – adventitia, M – media, I – intima. A. Optical section through the adventitia showing wavy collagen punctuated by thin elastic fibres. B. Reconstruction of a section along the central vessel axis, showing thick, longitudinally aligned elastic fibres of the IEL. C. Axial section. D. 3D section of the imaged region of the vessel. Bars 50 μm.

Figure 2. False colour images of the vessel pictured in Figure 1, raised to a transmural pressure of 30 mmHg causing the lumen to dilate to a diameter of 172 μm. Red labels: A – adventitia, M – media, I – intima. A. Optical section through the adventitia, showing a visually relatively unchanged fibrous matrix. B. Reconstruction of a section along the central vessel axis. Gaps caused by intimal dilation appear between the elastic fibres of the IEL, which in places bulge apart, braced by thinner connecting fibres. C. Axial section. D. 3D section of the imaged region of the vessel. Bars 50 μm.

Figure 3. False colour images of the distribution of elastin (green), collagen (blue) and cell nuclei stained with DAPI (red) of a vessel at 30 mmHg transmural pressure with a 268 μm lumen diameter. Yellow labels: A – adventitia, M – media, I – intima. A. section through the adventitia, showing adventitial, textured collagen and cell nuclei. B. Section through the adventitia and media, showing slender VSMC nuclei. C. Section through the adventitia, media and intima, showing the IEL and longitudinally aligned endothelial nuclei. D. Section through the wall and lumen. Bars 50 μm.

Figure 4. Variations in morphology of vessels. A. Axial optical section of a large vessel exhibiting wall thinning (arrow). B. Optical section of adventitia of an atypical vessel with significantly increased elastic fibre content. C. Axial optical section through a vessel undergoing myogenic contraction, exhibiting a crinkled IEL. D. High zoom TPF image of an elastin fibre located between two VSMCs. Bars A-C 50 μm, D window 25 μm.

Figure 5. Mechanics data. A: Elastic moduli assuming a layered vessel wall (E_m media modulus, E_a adventitia stiffness), and a homogeneous wall (E_h). Statistical significance: * $p<0.05$, ** $p<0.01$. B: Volumetric strains in the vessel walls. C: Peak circumferential stress in each layer analysed for the vessel depicted in Figures 1 and 2, with increasing transmural pressure. D: Ratio of adventital circumferential stress ($\sigma_{\theta a}$) to medial circumferential stress ($\sigma_{\theta m}$) at 30 mmHg transmural pressure with increasing lumen diameter. The positive trend indicates that the adventitia experiences proportionally greater wall stress in larger vessels.

Figure 6. Orientation distributions of the three fibrous networks.

Video Captions

Each video shows a sequence of optical sections starting at the peripheral adventitia and moving through the vessel wall into the lumen. The sequence is additive, so at the end of the video the whole imaged region is shown in 3D. Increments are 1 μm.

Video 1A. SHG (collagen) from the vessel depicted in Figures 1 and 2, at 3 mmHg transmural pressure. Field of view 250 μm.

Video 1B. TPF (elastic fibres and cellular fluorescence) from the vessel depicted in Figures 1 and 2, at 3 mmHg transmural pressure. Field of view 250 μm.

Video 1C. SHG (collagen) from the vessel depicted in Figures 1 and 2, at 30 mmHg transmural pressure. Field of view 250 μm.

Video 1D. TPF (elastic fibres and cellular fluorescence) from the vessel depicted in Figures 1 and 2, at 30 mmHg transmural pressure. Field of view 250 μm.

Video 2A. SHG (collagen) from the vessel depicted in Figure 3 at 2× zoom and 3 mmHg transmural pressure. Field of view 125 μm.

Video 2B. TPF (elastic fibres and cellular fluorescence) from the vessel depicted in Figure 3 at 2× zoom and 3 mmHg transmural pressure. Field of view 125 μm.

Video 2C. SHG (collagen) from the vessel depicted in Figure 3 at 2× zoom and 30 mmHg transmural pressure. Field of view 125 μm. Small zig-zags in fibres are an imaging artefact.

Video 2D. TPF (elastic fibres and cellular fluorescence) from the vessel depicted in Figure 3 at 2× zoom and 30 mmHg transmural pressure. Field of view 125 μm. Small zig-zags in fibres are an imaging artefact.

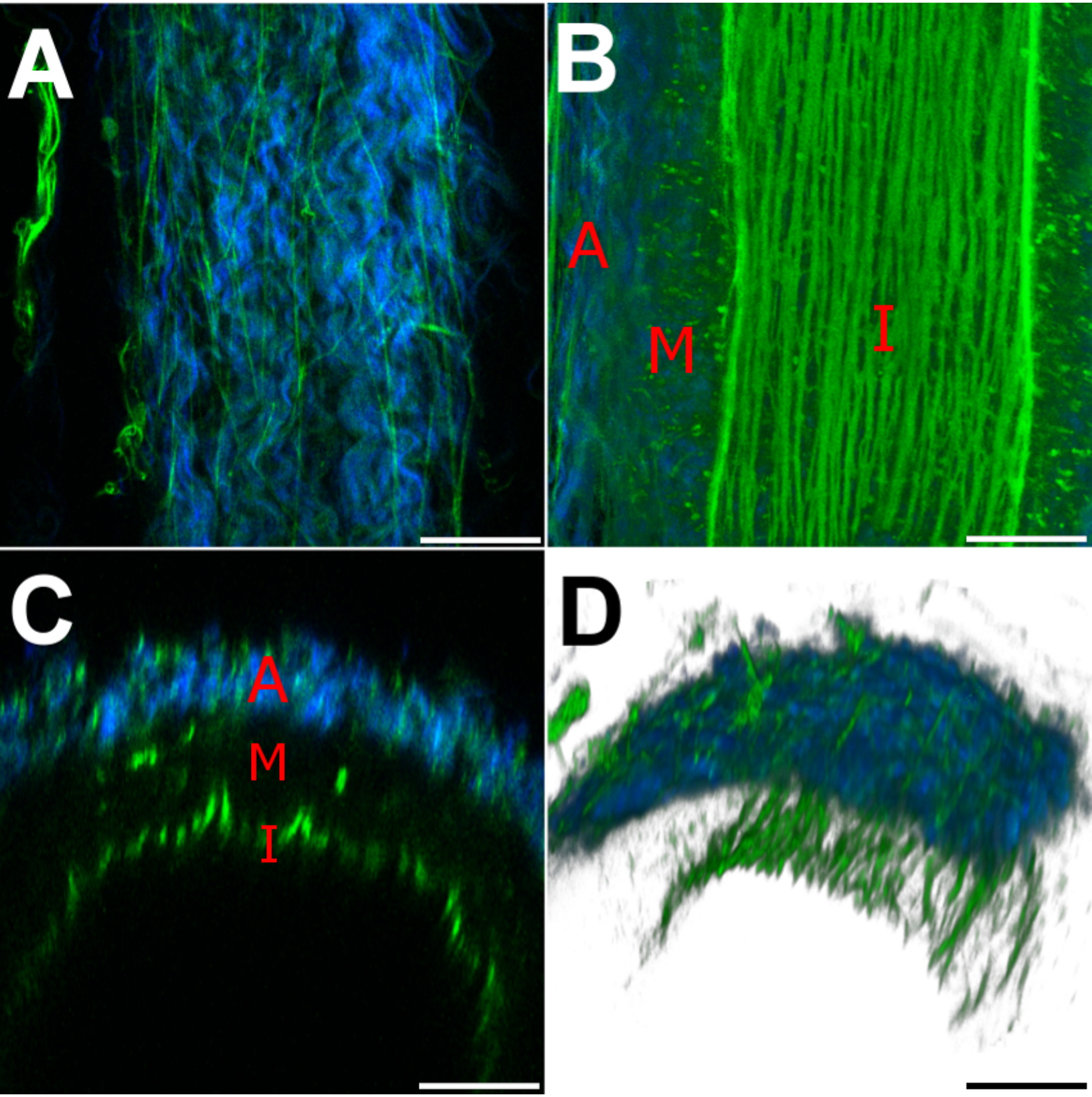
A
B
A
M
I
C
A
M
I
D

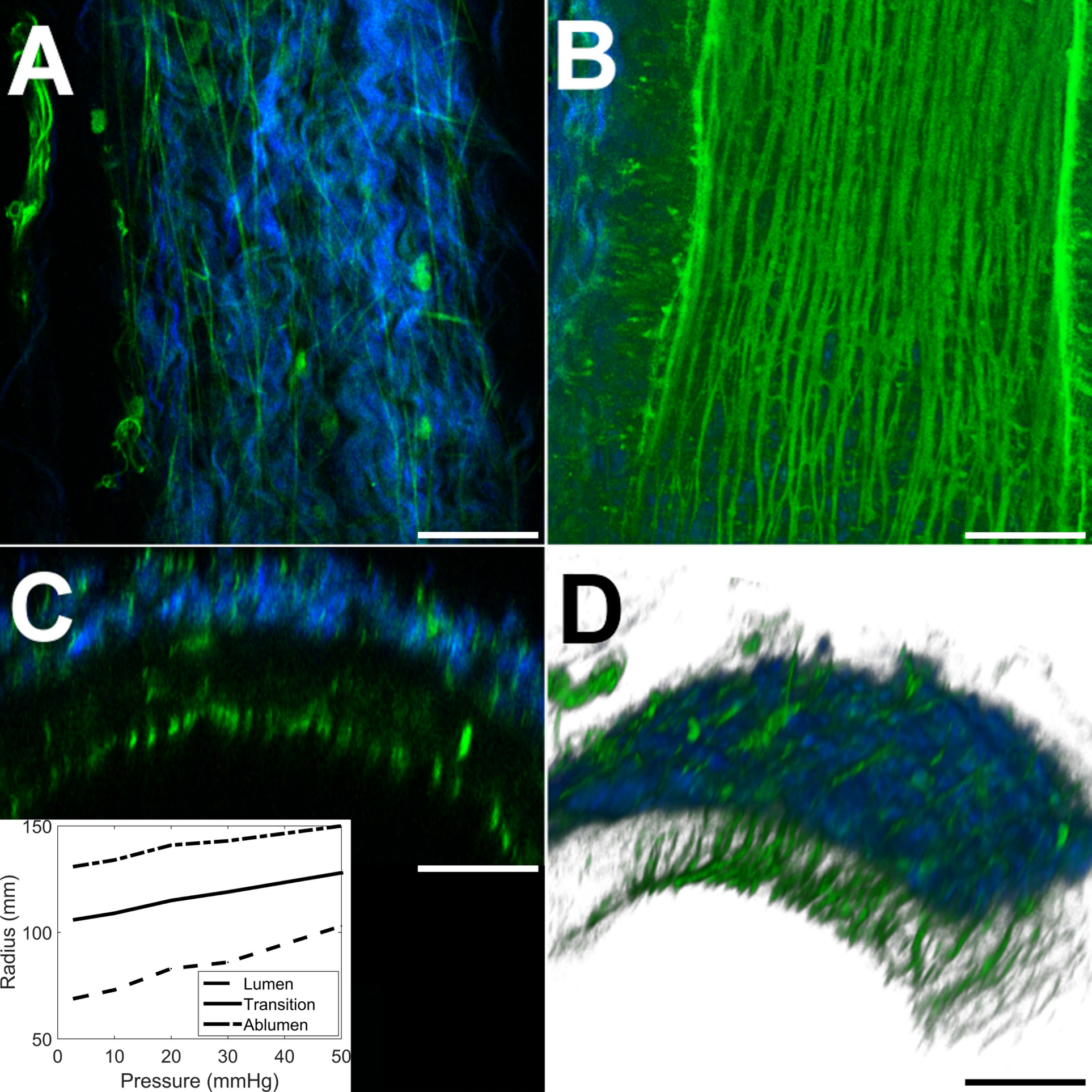
A
B
C
D
150
100
50
Radius (mm)
0
10
20
30
40
50
Pressure (mmHg)
Lumen
Transition
Ablumen

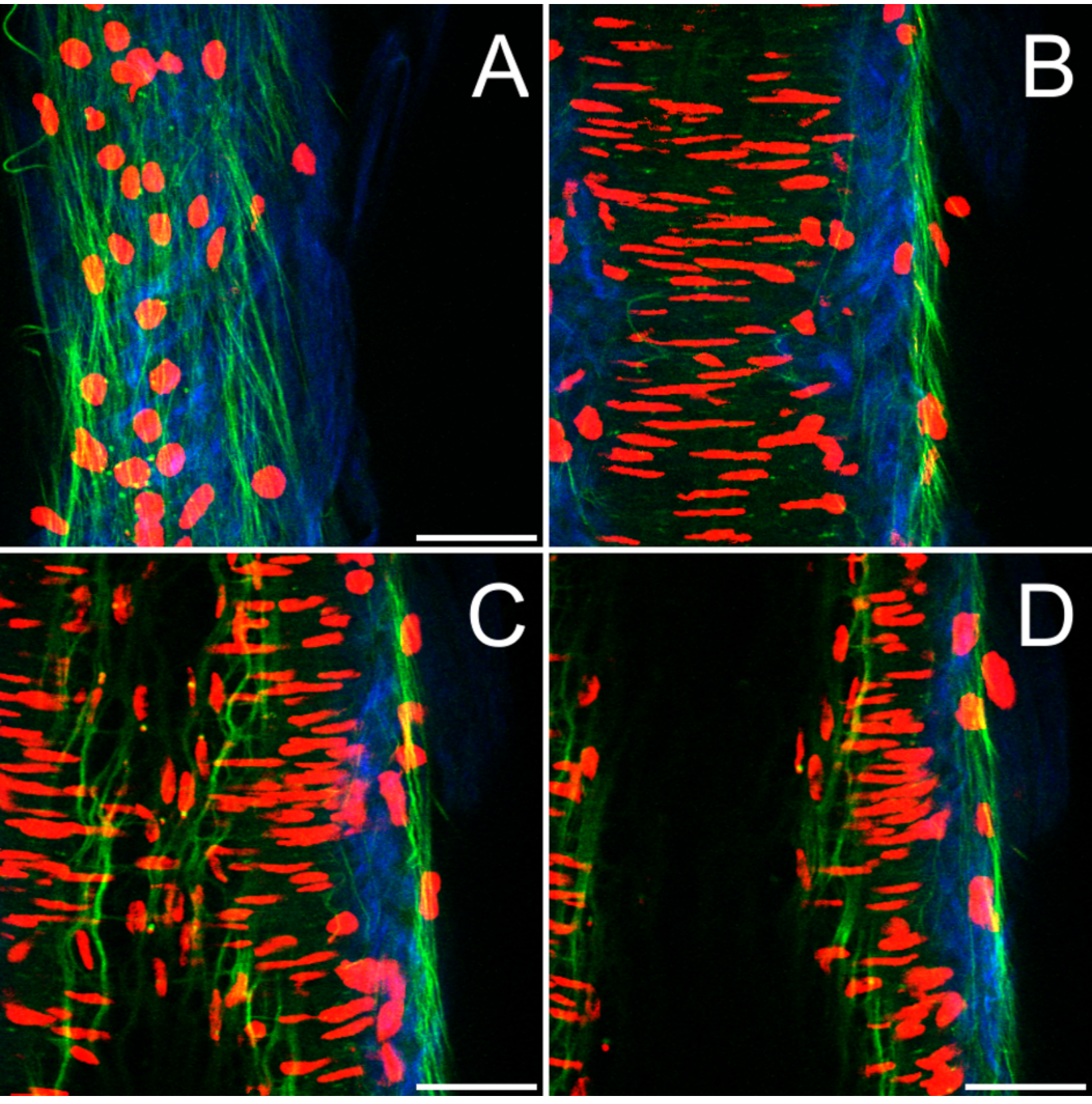
A
B
C
D

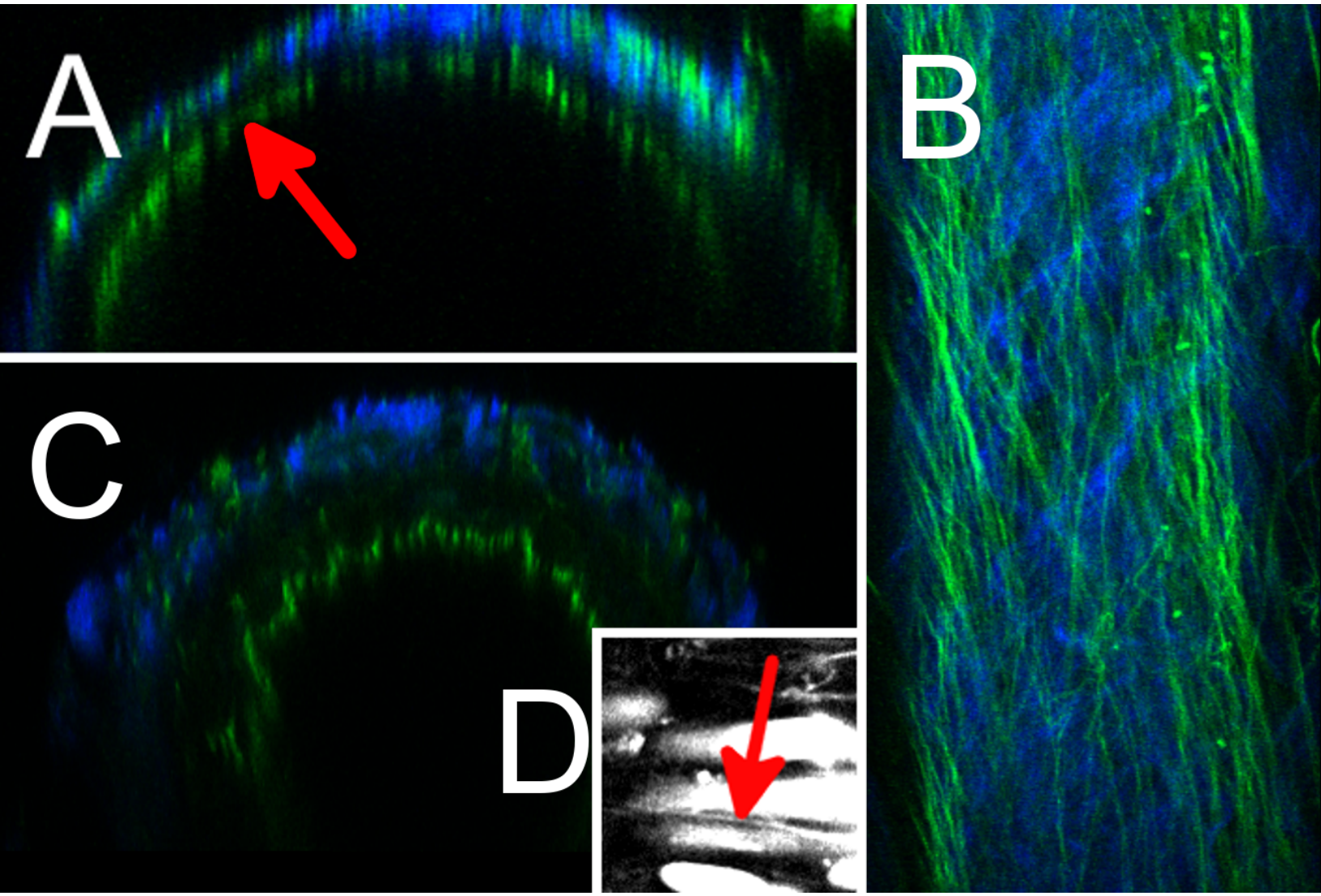
A
B
C
D

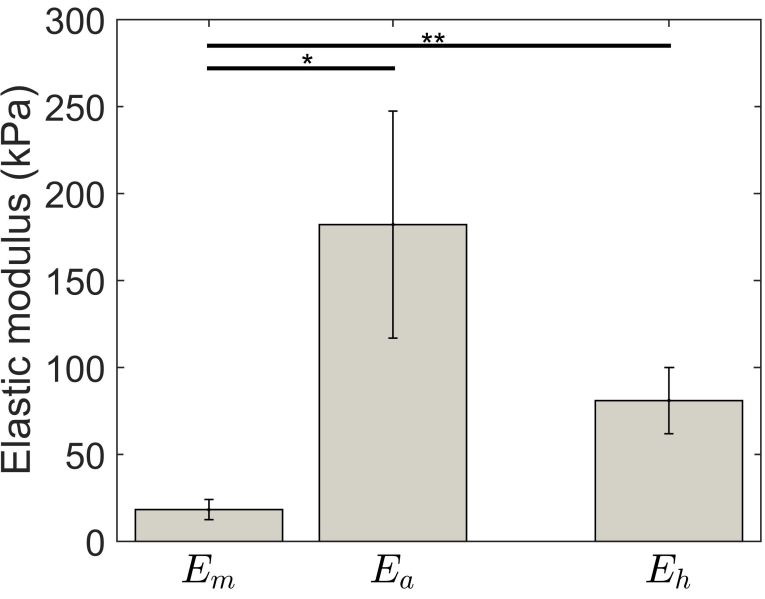
Elastic modulus (kPa)
300
250
200
150
100
50
0
*
**
E_m
E_a
E_h

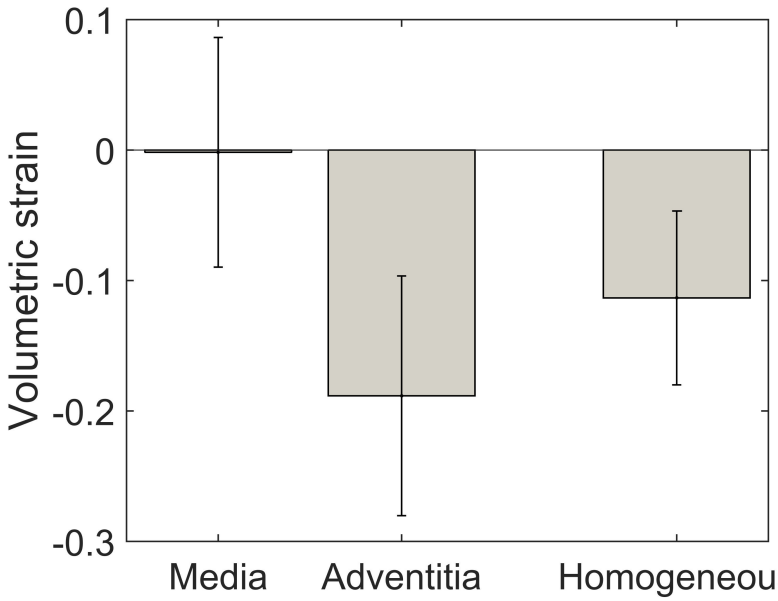
Volumetric strain
0.1
0
-0.1
-0.2
-0.3
Media
Adventitia
Homogeneous

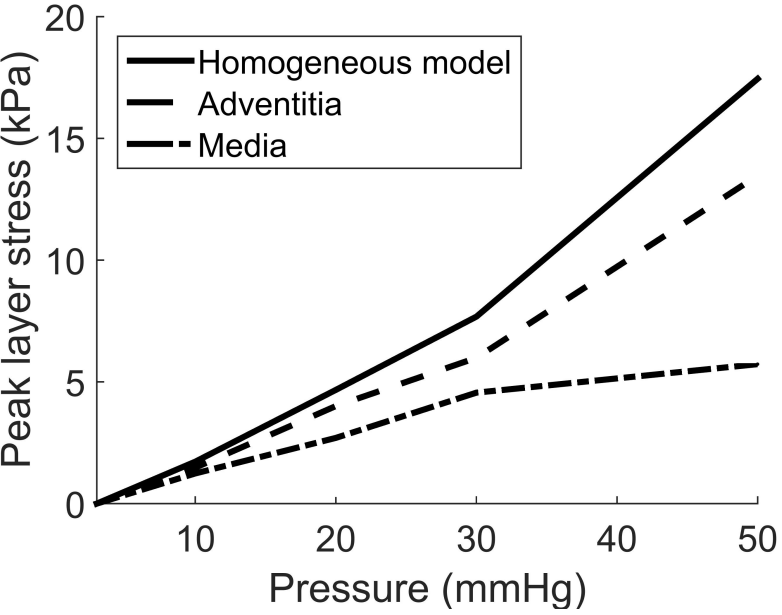
Peak layer stress (kPa)
20
15
10
5
0
Homogeneous model
Adventitia
Media
10
20
30
40
50
Pressure (mmHg)

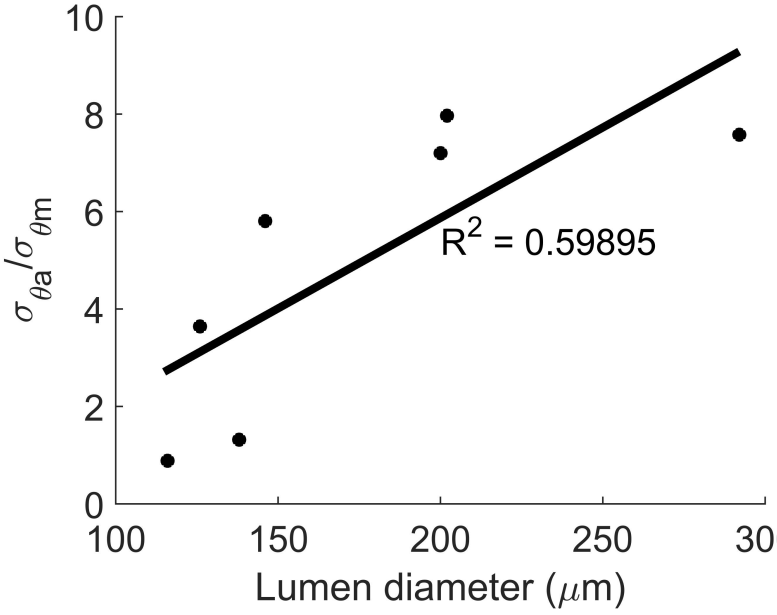
$\sigma_{\theta a}/\sigma_{\theta m}$
10
8
6
4
2
0
R^2 = 0.59895
100
150
200
250
300
Lumen diameter (μm)

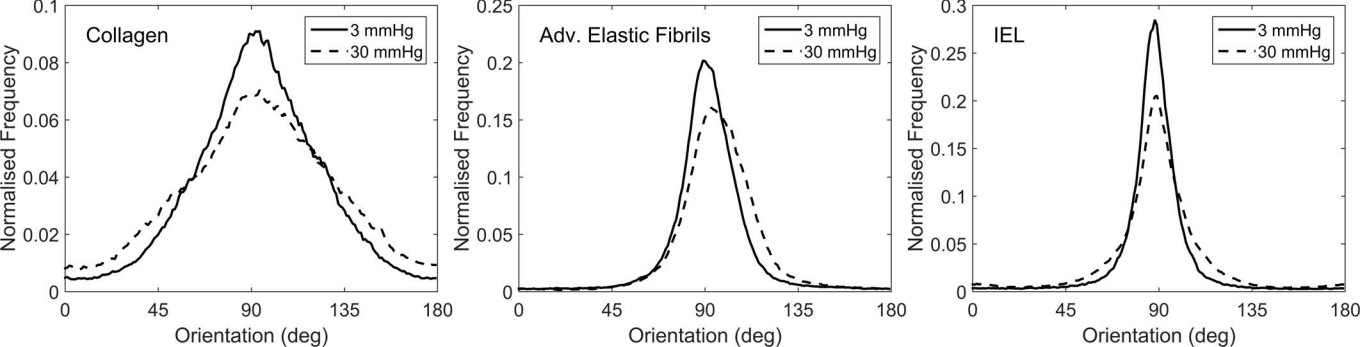
Collagen
3 mmHg
30 mmHg
Normalised Frequency
Orientation (deg)
0.1
0.08
0.06
0.04
0.02
0
0
45
90
135
180
Adv. Elastic Fibrils
3 mmHg
30 mmHg
Normalised Frequency
Orientation (deg)
0.25
0.2
0.15
0.1
0.05
0
0
45
90
135
180
IEL
3 mmHg
30 mmHg
Normalised Frequency
Orientation (deg)
0.3
0.25
0.2
0.15
0.1
0.05
0
0
45
90
135
180